JOURNAL OF SOLID STATE CHEMISTRY 93, 291–297 (1991)

Synthesis, Structure, and Physical Properties of the New Group IV Ternary Tellurides, Cu_2MTe_3 (M = Ti, Zr, Hf)

PATRICIA M. KEANE AND JAMES A. IBERS

Department of Chemistry, Northwestern University, Evanston, Illinois 60208-3113

Received October 30, 1990; in revised form March 11, 1991

The new close-packed compounds Cu_2TiTe_3, Cu_2ZrTe_3, and Cu_2HfTe_3 have been prepared through direct reactions of the elements. The compounds crystallize in space group C_{2h}^3–$C2/m$ of the monoclinic system with four formula units in cells of dimensions a = 19.73(3), b = 3.970(4), c = 7.076(4) Å, β = 95.7(1)° (T = 153 K) for Cu_2TiTe_3; a = 20.288(4), b = 4.065(2), c = 7.250(1) Å, β = 97.32(2)° (T = 153 K) for Cu_2ZrTe_3; a = 20.188(6), b = 4.054(1), c = 7.216(2) Å, β = 97.16(1)° (T = 111 K) for Cu_2HfTe_3. The Cu_2HfTe_3 structure has been solved by single crystal X-ray methods. The final R index on F_0^2 for 1509 unique observations and 20 variables is 0.048. The Cu_2HfTe_3 structure is composed of distorted tetrahedral Cu atoms and distorted octahedral Hf atoms coordinated by Te atoms. These polyhedra are linked together through edge and face sharing. As there are no short Te···Te interactions the Cu atoms are in the +1 oxidation state and the Hf atoms are in the +4 oxidation state. The metal–metal interactions between the Cu atoms and the Hf and both Cu atoms form six-membered rings. These rings interconnect to create arsenic-like buckled sheets that run parallel to $(\bar{2}01)$. Electrical resistivity measurements indicate that Cu_2HfTe_3 and Cu_2ZrTe_3 are metals with $\rho_{286} \approx 3.8 \times 10^{-4}$ Ω cm and 2.0×10^{-3} Ω cm, respectively. Cu_2ZrTe_3 exhibits Pauli-paramagnetic behavior with $\chi \approx 3.5 \times 10^{-4}$ emu mol^{-1}.

Introduction

The binary and ternary transition metal chalcogenides are particularly interesting because of their important physical properties and novel structural motifs. There has been extensive exploration of the $M_xM'_yQ_z$ system, where M = Nb or Ta; M' = Ni, Pd, Pt; and Q = S, Se, Te for new compounds (*1–10*). Although a number of the Group V ternary tellurides have been discovered (*6–10*), there have been no Group IV ternary tellurides synthesized.

Since the discovery of the utility of reactive fluxes in the synthesis of ternary alkali metal–transition metal chalcogenides (*11*), there has been an increased interest in the use of these melts to produce ternary chalcogenides (*12–15*), many of which turn out to exhibit unprecedented structures. This synthetic technique exploits the typically low melting mixtures A_2Q/Q (A = alkali metal, Q = S, Se, Te) not only to reduce the melting temperature of the reaction, but to act as an alkali metal and chalcogen donor. The Cu_xTe_y (*16*) phases, similar to the A_xTe_y (*17, 18*) phases, exhibit a low melting region between approximately 50 and 100% Te. We report with the synthesis of Cu_2MTe_3 (M = Ti,Zr,Hf) that this molten flux technique can be extended to include A = Cu. Here we present the synthesis of

0022-4596/91 $3.00

the new solid state Group IV tellurides Cu_2MTe_3 (M = Ti,Zr,Hf), the resistivity for M = Zr,Hf, the magnetic susceptibility for M = Zr, and the structure for M = Hf.

Experimental

Synthesis. Powders of elemental Cu (AESAR, 99.999%), Hf (AESAR, 99.6%), and Te (AESAR, 99.5%) were combined in an atomic ratio of 4 : 1 : 6, respectively, ground together, and loaded into a quartz tube. The tube was then evacuated ($\sim 10^{-4}$ Torr) and sealed. It was heated in a furnace at 650°C for 6 days, then ramped to 900°C to heat for 4 days. The furnace was cooled at the rate of 3°C/hr to 450°C and then to room temperature at 90°C/hr. The product consisted of shiny black needle-shaped crystals of Cu_2HfTe_3 formed within a melt. Single crystals suitable for physical measurements and X-ray diffraction studies were extracted manually from the melt. Cu_2ZrTe_3 was prepared in an analogous manner with the Cu, Zr (AESAR, 99%), and Te powders in the same ratio. The product contained shiny, silver needles formed in a melt and dull black needles (in very low yield) of $Cu_{1.85}Zr_2Te_6$. The stoichiometry of this second zirconium-containing ternary phase was determined by single crystal X-ray studies (*19*). Cu_2TiTe_3 was prepared by reaction of Cu, Ti (ALFA, 99.9%), and Te powders in a 3 : 1 : 7 ratio. The silver shiny needles of the ternary phase were embedded in a melt. These four compounds are air stable.

Qualitative chemical analysis of the primary phases with the microprobe of a Hitachi-S570 scanning electron microscope confirmed the presence of (Cu, Hf, Te), (Cu, Zr, Te), and (Cu, Ti, Te) in the approximate ratios of (1.5 : 1.0 : 2.5), (3.5 : 1.0 : 4.0), and (2.0 : 1.0 : 2.8), respectively. The exact composition of the Hf compound was determined from the crystal structure determination.

Resistivity. Single crystals ranging in length from 1.0 to 1.8 mm of Cu_2ZrTe_3 and Cu_2HfTe_3 were mounted with Ag paint on Al wires (with graphite fiber extensions) of an integrated circuit chip. The mounted single crystals were then checked by EDAX measurements to confirm their composition. Four probe ac resistivity measurements along b, the needle axis, were made following procedures described previously (*20*).

Magnetic susceptibility. Cu_2ZrTe_3 single crystals (5.4 mg) were selected for measurement. The composition of 14 of these crystals was checked by EDAX measurements and found to confirm the composition Cu_2ZrTe_3. Variable-temperature magnetic susceptibility measurements were made between 4.5 and 296 K at a magnetic field strength of 5 kG with a Quantum Design SQUID magnetometer. The magnetic moment was corrected for background contribution from the sample holder. The magnetization of Cu_2ZrTe_3 was linearly proportional to the applied field at 296 K. The data were corrected for ion-core diamagnetic contributions for Cu^{+1}, Zr^{+4}, and Te^{-2} (*21*) to obtain the molar susceptibilities.

Structure determination for Cu_2ZrTe_3 and Cu_2TiTe_3. The cell parameters (a = 20.288(4), b = 4.065(2), c = 7.250(1) Å, β = 97.32(2)°) of a single crystal of Cu_2ZrTe_3 were determined from a least-squares analysis of 24 automatically centered reflections in the range $20° \leq \theta (CuK\alpha_1) \leq 44°$ on an Enraf–Nonius CAD4 diffractometer at 153 K. Similarly, the cell parameters of Cu_2TiTe_3 (a = 19.73(3), b = 3.970(4), c = 7.076(4) Å, β = 95.7(1)°) were determined from 13 reflections in the range $12° \leq \theta(CuK\alpha_1) \leq 25$. Systematic absences indicated monoclinic symmetry and were consistent with space group $C2/m$.

Structure determination for Cu_2HfTe_3. Weissenberg photographs established the monoclinic symmetry and approximate cell parameters. The reflection conditions (hkl, $h + k = 2n$; $h0l$, $h = 2n$; and $0k0$, $k = 2n$) are consistent with space groups C_2^3–$C2$, C_s^3–Cm, and C_{2h}^3–$C2/m$. The lattice con-

stants were determined from a least-squares analysis of the setting angles of 17 reflections in the range of $35° < 2\theta(MoK\alpha_1) < 39°$ that had been automatically centered at 111 K on a Picker FACS-1 diffractometer. Six standard reflections monitored every 100 reflections exhibited no significant fluctuation or decay during data collection. Crystal data and other crystallographic details are described in Table I.

Calculations were performed on a Stellar GS2000 computer with programs and methods standard for this laboratory (*22*). Conventional atomic scattering factors (*23*) were used and anomalous dispersion corrections (*24*) were applied. A satisfactory residual of 0.056 resulted when the absorption-corrected intensities were averaged in Laue group $2/m$. Thus the centrosymmetric space group $C2/m$ was chosen. All of the atomic positions were found with the use of the direct methods program SHELX-86 (*25*). The model was restricted to isotropic thermal motion. The final refinement on F_0^2 involved 20 variables and 1509 unique data, including those for which $F_0^2 \leq 0$. A final electron density map reveals no features greater than 2.7% the height of a Cu atom. An analysis of $\Sigma w(F_0^2 - F_c^2)^2$ as a function of F_0^2, Miller indices, and setting angles shows no uncommon trends. Final positional and thermal parameters are provided in Table II. The thermal parameters are reasonable and there is no indication of nonstoichiometry or substitutional disorder. A list of structure amplitudes is available.[1]

TABLE I

DATA COLLECTION AND REFINEMENT DETAILS FOR Cu_2HfTe_3

Formula	Cu_2HfTe_3
Fw	688.38
Space group	C_{2h}^3–$C2/m$
a (Å)	20.188(6)
b (Å)	4.054(1)
c (Å)	7.216(2)
β (deg)	97.16(1)
Vol (Å^3)	586(1)
Z	4
T of data collection (K)	111[a]
Density (calcd; g cm^{-3})	7.81
Crystal volume (mm^3)	2.3×10^{-4}
Crystal shape	Needle with rectangular cross section bound by {001}, {100}, {010}
Radiation	Graphite monochromated Mo$K\alpha$ ($\lambda(K\alpha_1)$ = 0.7093 Å)
Linear absorption coefficient (cm^{-1})	394
Transmission factors	0.21–0.47[b]
Takeoff angle (deg)	2.5
Receiving aperture (mm)	Horizontal, 3.8; vertical, 3.7; 32 cm from crystal
Scan type	θ–2θ
Scan range in 2θ	0.5° below $K\alpha_1$ to 1.0° above $K\alpha_2$
Background counts	10 sec at each end of scan with rescan option[c]
2θ limits (deg)	$2.0 \leq 2\theta(MoK\alpha_1) \leq 71.0$
Data collected	$\pm h, \pm k, \pm l$
No. of unique data	1509
p factor	0.04
Final number of variables	20
$R(F^2)$	0.048
$R_w(F^2)$	0.073
$R(F)$ for $F_0^2 > 3\,\sigma(F_0^2)$	0.034
Error in observation of unit weight	1.32

[a] The low temperature system is based on a design by J. C. Huffman, Ph.D. thesis, Indiana University, 1974.

[b] The analytical method was used for the absorption correction (J. de Meulenaer and H. Tompa, *Acta Crystallogr.* **19**, 1014, 1965).

[c] The diffractometer was operated under the Vanderbilt disk oriented system (P. G. Lenhert, *J. Appl. Crystallogr.* **8**, 568, 1975).

[1] See NAPS document No. 04862 for 8 pages of supplementary materials. Order from ASIS/NAPS. Microfiche Publications, P.O. Box 3513, Grand Central Station, New York, NY 10163. Remit in advance $4.00 for microfiche copy or $7.75 for photocopy. All orders must be prepaid. Institutions and Organizations may order by purchase order. However, there is a billing and handling charge for this service of $15. Foreign orders add $4.50 for postage and handling, $1.50 for postage of any microfiche orders.

TABLE II

POSITIONAL PARAMETERS AND ISOTROPIC THERMAL PARAMETERS FOR Cu_2HfTe_3

Atom	x	y	z	B^a(Å^2)
Hf[b]	0.353750(11)	0	0.945440(33)	0.486(6)
Te(1)	0.248328(17)	0	1.214784(50)	0.395(7)
Te(2)	0.417792(18)	0	0.632612(52)	0.460(7)
Te(3)	0.416719(18)	$-\frac{1}{2}$	1.179629(53)	0.447(7)
Cu(1)	0.287865(39)	0	0.57071(11)	0.63(1)
Cu(2)	0.452916(39)	$-\frac{1}{2}$	0.84751(11)	0.59(1)

[a] $B = 8\pi^2 \langle u^2 \rangle$, where $\langle u^2 \rangle$ is the mean-square displacement.
[b] All atoms are on site symmetry m and Wyckoff position i.

Results and Discussion

Description of the structure. Metrical details for the Cu_2HfTe_3 structure are summarized in Table III. A stereoview of the structure down [001] is shown in Fig. 1. The atom labeling scheme and a perspective drawing of the structure viewed down [010] are provided in Fig. 2.

This compound crystallizes in a new three-dimensional structure that has hexagonal closest packed layers of Te atoms extending orthogonal to [100]. The filling of the somewhat distorted octahedral and tetrahedral vacancies is unusual. In two-thirds of the layers one-half the octahedral sites are occupied by Hf atoms, in one-third of the layers one-half the tetrahedral sites are filled by Cu(2) atoms, and in the other two-thirds of the layers one-quarter of the tetrahedral sites are filled by Cu(1) atoms (Fig. 3).

TABLE III

SELECTED BOND DISTANCES (Å) AND ANGLES (deg) FOR Cu_2HfTe_3

Hf–Te(2)	2.736(1)	Te(2)–Hf–Te(3)	105.60(1)
Hf–2Te(3)	2.838(1)	Te(2)–Hf–Te(1)	93.06(2)
Hf–2Te(1)	3.018(1)	Te(2)–Hf–Te(1)	164.20(1)
Hf–Te(1)	3.053(1)	Te(3)–Hf–Te(3)	91.16(2)
Hf–Cu(1)	2.864(1)	Te(3)–Hf–Te(1)	89.05(2)
Hf–2Cu(2)	2.994(1)	Te(3)–Hf–Te(1)	85.25(2)
Cu(1)–Te(1)	2.594(1)	Te(1)–Cu(1)–Te(2)	110.53(3)
Cu(1)–Te(2)	2.606(1)	Te(1)–Cu(1)–Te(1)	119.64(2)
Cu(1)–2Te(1)	2.705(1)	Te(2)–Cu(1)–Te(2)	103.81(2)
Cu(1)–2Cu(1)	2.665(1)	Te(3)–Cu(2)–Te(2)	117.72(2)
Cu(2)–Te(3)	2.590(1)	Te(3)–Cu(2)–Te(3)	117.49(3)
Cu(2)–2Te(2)	2.597(1)	Te(2)–Cu(2)–Te(3)	98.97(2)
Cu(2)–Te(3)	2.663(1)	Te(2)–Cu(2)–Te(2)	102.58(4)
Cu(2)–Cu(2)	2.726(2)	Cu(1)–Hf–Cu(2)	91.36(2)
		Cu(1)–Hf–Hf	90
		Cu(2)–Hf–Cu(2)	85.22(3)
		Cu(1)–Cu(1)–Cu(1)	99.00(5)
		Cu(1)–Cu(1)–Hf	122.67(3)
		Cu(1)–Cu(1)–Cu(1)	139.50(3)
		Cu(2)–Cu(2)–Hf	103.28(4)

There are three basic subunits in the structure (Fig. 3). The first is the **A** slab in which one-half the tetrahedral sites are occupied by Cu(2) atoms. This slab is composed of four close-packed and tightly bound layers Te–Cu(2)–Cu(2)–Te. Within slab **A**, each Cu(2) atom has one Cu(2) metal neighbor in the adjacent layer at a distance of 2.726(2) Å. The Cu(2) atoms are coordinated by Te atoms in distorted tetrahedral coordination. These Cu(2) tetrahedra are edge sharing.

The second and third subunits, **B** and **C**, are related by a two-fold rotation along the b axis followed by the C-centering operation. In these slabs, one-half of the octahedral and one-quarter of the tetrahedral sites are filled. The Hf atoms are at the centers of distorted octahedra and the Cu(1) atoms are at the centers of distorted tetrahedra of Te atoms. The octahedra of the Hf atoms and the tetrahedra of the Cu(1) atoms are

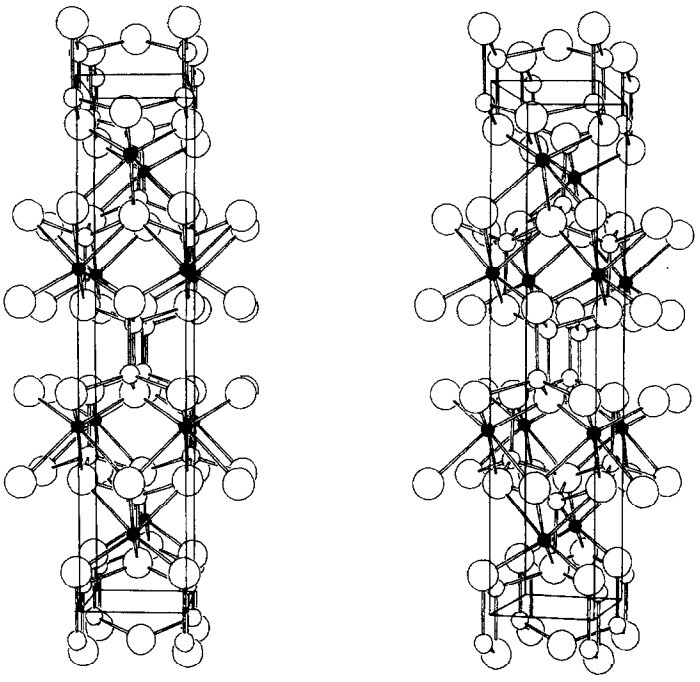

FIG. 1. Stereoview of Cu_2HfTe_3 down [001] with Cu–Te and Hf–Te interactions drawn. Hf atoms are filled circles, Cu atoms are medium open circles, Te atoms are large open circles. The a axis extends from bottom to top; the b axis extends from left to right.

face sharing. This connectivity results in a close interaction of 2.864(1) Å between the Cu(1) and Hf atoms. In the structures of hexagonally closest packed Cu and Hf metals the metal–metal distances are 2.556 (*26*) and 3.195 Å (*27*), respectively. Between the adjacent **B** and **C** subunits the tetrahedra of Cu(1) are edge sharing with a resultant Cu(1)–Cu(1) distance of 2.665(1) Å. Between subunits **A** and **B** and subunits **A** and **C**, each Hf octahedron shares edges with two Cu(2) tetrahedra. This leads to a short Hf–Cu(2) interaction of 2.994(1) Å. This is somewhat longer than the Hf–Cu(1) distance (2.864(1) Å), possibly indicating a weaker metal–metal interaction between atoms in different layers.

The four metal–metal interactions (Hf–Cu(1), Hf–Cu(2), Cu(1)–Cu(1), and Cu(2)–Cu(2)) interconnect to form sheets of buckled, six-membered rings that extend parallel to $(\bar{2}01)$. These sheets, which form arsenic-like layers, are shown in Fig. 4 with only the metal–metal interactions drawn. These sheets can be viewed as a fusion of cyclohexane-like rings of chair conformation. One ring is composed of four Cu(2) and two Hf atoms; the other is composed of three Cu(1), one Cu(2), and two Hf atoms.

As there are no short Te···Te interactions in this structure, the Te atoms may be assigned a formal oxidation state of -2. The coordination geometries around the Cu and Hf atoms are consistent with the assignment of formal oxidation states of $+1$ and $+4$, respectively, although in view of the metallic nature of the compound (vide infra) these formal oxidation states are an oversimplification. It is interesting that in the reaction Hf has been fully oxidized while Cu has not.

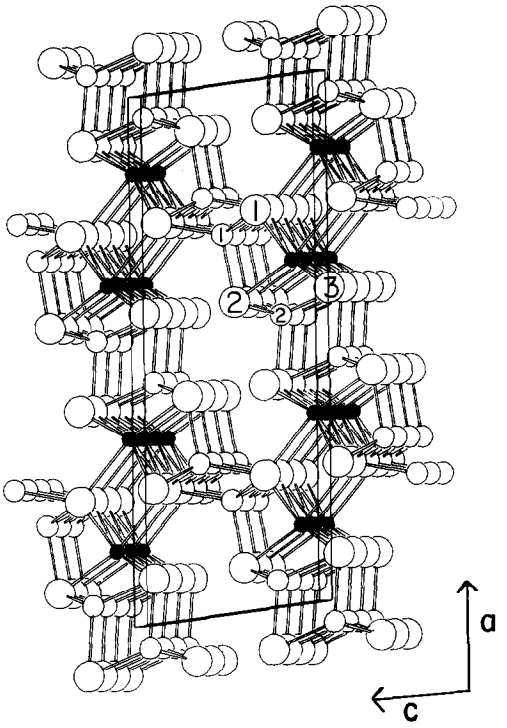

FIG. 2. Perspective view down [010] of Cu_2HfTe_3, with Cu–Te and Hf–Te interactions drawn. The small solid circles are Hf atoms; open medium circles are Cu atoms; large open circles are Te atoms.The labeling scheme is shown.

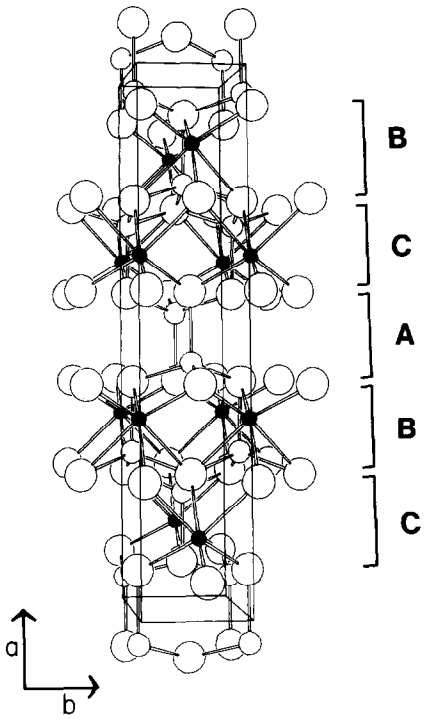

FIG. 3. View of Cu_2HfTe_3 down [001] with subunits labeled. Hf atoms are filled circles, Cu atoms are medium open circles, Te atoms are large open circles.

As Cu_2TiTe_3, Cu_2ZrTe_3, and Cu_2HfTe_3 show the same systematic absences and crystallize in cells of similar dimensions we believe they are isostructural.

Resistivity and magnetic susceptibility. Four-probe ac resistivity along the needle axis, *b*, shows that Cu_2HfTe_3 and Cu_2ZrTe_3 are metals with $\rho_{286} \approx 3.8\ 10^{-4}$ and $2.0\ 10^{-3}$ Ω cm, and $\rho_5 \approx 2.3\ 10^{-4}$ and $1.8\ 10^{-3}$ Ω cm, respectively. A plot of the electrical resistivity behavior over the temperature range 5–286 K is given in Fig. 5. The behavior is consistent with metallic conductors. The temperature dependence of the resistivity for both materials is nearly linear. As expected for a metallic conductor, Cu_2ZrTe_3 shows temperature-independent Pauli-para-

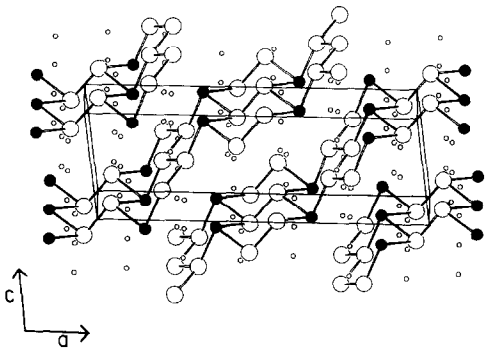

FIG. 4. Drawing of layers of metal atoms parallel to $(\bar{2}01)$, with Cu–Cu and Cu–Hf interactions drawn. Small unfilled circles are Te atoms; medium filled circles are Hf atoms; large open circles are Cu atoms.

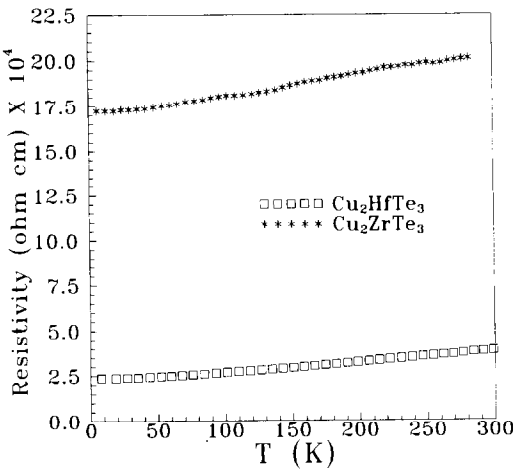

FIG. 5. Electrical resistivity (ohm cm) vs temperature as measured along the needle axis, b, for Cu_2HfTe_3 and Cu_2ZrTe_3.

magnetism with a susceptibility of approximately 3.5×10^{-4} emu mol^{-1}.

Band structure calculations might prove useful in understanding the metallic behavior of these compounds.

Acknowledgments

This research was supported by the U.S. National Science Foundation through Grant DMR88-13623. This work made use of Central Faclities supported by the National Science Foundation through the Northwestern University Materials Research Center, Grant DMR88-21571.

References

1. D. A. KESZLER AND J. A. IBERS, *J. Solid State Chem.* **52,** 73 (1984).
2. D. A. KESZLER AND J. A. IBERS, *J. Am. Chem. Soc.* **107,** 8119 (1985).
3. D. A. KESZLER, P. J. SQUATTRITO, N. E. BRESE, J. A. IBERS, M. SHANG, AND J. LU, *Inorg. Chem.* **24,** 3063 (1985).
4. S. A. SUNSHINE AND J. A. IBERS, *Inorg. Chem.* **24,** 3611 (1985).
5. S. A. SUNSHINE AND J. A. IBERS, *Inorg. Chem.* **25,** 4355 (1986).
6. S. A. SUNSHINE, D. A. KESZLER, AND J. A. IBERS, *Acc. Chem. Res.* **20,** 395 (1987).
7. E. W. LIIMATTA AND J. A. IBERS, *J. Solid State Chem.* **71,** 384 (1987).
8. E. W. LIIMATTA AND J. A. IBERS, *J. Solid State Chem.* **77,** 141 (1988).
9. E. W. LIIMATTA AND J. A. IBERS, *J. Solid State Chem.* **78,** 7 (1989).
10. A. MAR AND J. A. IBERS, *J. Solid State Chem.*, in press.
11. S. A. SUNSHINE, D. KANG, AND J. A. IBERS, *J. Am. Chem. Soc.* **109,** 6202 (1987).
12. P. M. KEANE AND J. A. IBERS, *Inorg. Chem.*, **30,** 1327 (1991).
13. Y. PARK AND M. G. KANATZIDIS, *Angew. Chem. Int. Ed. Eng.* **29,** 914 (1990).
14. M. G. KANATZIDIS AND Y. PARK, *J. Am. Chem. Soc.* **111,** 3767 (1989).
15. D. KANG AND J. A. IBERS, *Inorg. Chem.* **27,** 549 (1988).
16. T. B. MASSALSKI (Ed.), "Binary Alloy Phase Diagrams," Vol. I, pp. 967–968, American Society for Metals, Metals Park, Ohio (1986).
17. T. B. MASSALSKI (Ed.), "Binary Alloy Phase Diagrams," Vol. II, pp. 1671, 1673, American Society for Metals, Metals Park, Ohio (1986).
18. T. B. MASSALSKI (Ed.), "Binary Alloy Phase Diagrams," Vol. I, pp. 904–905, American Society for Metals, Metals Park, Ohio (1986).
19. P. M. KEANE AND J. A. IBERS, *Inorg. Chem.*, in press.
20. T. E. PHILLIPS, J. R. ANDERSON, C. J. SCHRAMM, AND B. H. HOFFMAN, *Rev. Sci. Instrum.* **50,** 263 (1979).
21. L. N. MULAY AND E. A. BOUDREAUX, Eds., "Theory and Application of Molecular Diamagnetism," Wiley–Interscience, New York (1976).
22. J. M. WATERS AND J. A. IBERS, *Inorg. Chem.* **16,** 3273 (1977).
23. J. A. IBERS AND W. C. HAMILTON (Eds.), "International Tables for X-ray Crystallography," Vol. IV, Tables 2.2A and 2.3.1, Kynoch Press, Birmingham (1974).
24. J. A. IBERS AND W. C. HAMILTON, *Acta Crystallogr.* **17,** 781 (1964).
25. G. M. SHELDRICK, *in* "Crystallographic Computing 3" (G. M. Sheldrick, C. Kruger, and R. Goddard, Eds.), pp. 175–189, Oxford Univ. Press, Oxford (1985).
26. W. E. KRULL AND R. W. NEWMAN, *J. Appl. Crystallogr.* **3,** 519 (1970).
27. R. B. RUSSELL, *J. Appl. Phys.* **24,** 232 (1953).